J. Fluid Mech. (2008), *vol.* 600, *pp.* 235–244.
doi:10.1017/S0022112008000554 Printed in the United Kingdom

Mixing efficiency in controlled exchange flows

TJIPTO PRASTOWO, ROSS W. GRIFFITHS, GRAHAM O. HUGHES AND ANDREW McC. HOGG

Research School of Earth Sciences, The Australian National University, Canberra, ACT 0200, Australia

(Received 4 October 2007 and in revised form 22 January 2008)

Turbulence and mixing are generated by the shear between two counter-flowing layers in hydraulically controlled buoyancy-driven exchange flows through a constriction. From direct measurements of the density distribution and the amount of turbulent mixing in steady laboratory exchange flows we determine the overall efficiency of the mixing. For sufficiently large Reynolds numbers the mixing efficiency is 0.11 ($\pm$0.01), independent of the aspect ratio and other details of constriction geometry, in good agreement with a scaling analysis. We conclude that the mixing in shear flows of this type has an overall efficiency significantly less than the maximum value widely proposed for stratified turbulence.

1. Introduction

The density-driven exchange of two fluids through a narrow constriction between two large reservoirs is generally unstable and a substantial amount of turbulent mixing between the counter-flowing layers takes place. It seems likely that similar shear instability and mixing also occur in density-driven exchange flows through channels and over sills between abyssal ocean basins, in straits between marginal seas and the oceans and in estuaries. Indeed, the amount of mixing resulting from flow through straits and over sills may account for substantial amounts of vertical mixing in the deep oceans (Bryden & Nurser 2003). Vertical mixing assists in maintaining the stratification in the face of broad upward displacement of water by the downwelling of dense currents (Munk & Wunsch 1998). This mixing will be distributed throughout the ocean depth and will occur near the bottom and side boundaries. The total amount of mixing is limited to the product of the power input to the oceans and the average mixing efficiency, the proportion of the turbulent kinetic energy that goes into irreversibly raising the potential energy stored in the density field (Peltier & Caulfield 2003).

Although here we will not be primarily concerned with the exchange transport, or with the application of internal hydraulic theory, we note that in the basic theory the flow is assumed to be immiscible, steady, inviscid, incompressible and hydrostatic (Wood 1970; Lawrence 1990). However, exchange flows in the ocean (e.g. Gregg & Özsoy 2002) and in the laboratory show significant differences from the predictions for the ideal case. Corrections to the two-layer theory to account for these differences have included time dependence (Helfrich 1995), friction (Gu & Lawrence 2005), non-hydrostatic effects (Zhu & Lawrence 1998) and mixing (Winters & Seim 2000; Hogg, Ivey & Winters 2001). In particular, laboratory measurements of two-layer exchange through a constriction show that mixing is responsible for reducing the net mass transport from the maximal hydraulic solution by about 20% (Helfrich 1995)

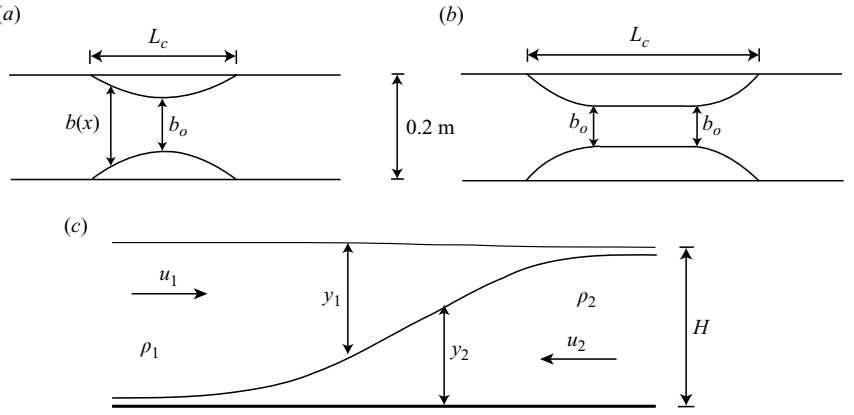

FIGURE 1. Plan diagrams of (*a*) the 'short constrictions' and (*b*) the 'long constriction', and (*c*) a vertical section of ideal two-layer exchange flow through a 'short' constriction (variables are defined in the text).

and numerical simulations indicate that mixing reduces volume transport by 15% (Winters & Seim 2000).

Surprisingly, there have been no previous measurements of the amount of mixing in exchange flows. However, it is necessary to know the amount of mixing in order to understand the rate of production of mixed water or the global contribution of exchange flows to vertical mixing. The observed shear instability in buoyancy-driven exchange flows may also provide insights into the dynamics of mixing relevant to other forms of unstable shear flows. In this study we use laboratory experiments to quantify the cumulative efficiency of mixing in the case of hydraulically controlled density-driven two-layer exchange flows through lateral constrictions (described in § 2). In § 3, we describe the methods and analysis, and in § 4, we show the results and develop a theoretical scaling analysis for the mixing efficiency.

2. Experiments

All experiments were carried out in a flat-bottomed tank 5.26 m long and 0.20 m wide. One of four symmetric inserts was placed at the centre of the channel to form a constriction. Three of the inserts had a sinusoidal shape so that the width of the channel varied smoothly with distance (figure 1*a*). The minimum width b_o of the constrictions was 20 mm, 60 mm or 100 mm and the total constriction length L_c was 0.6 m, 0.5 m or 0.4 m, respectively. The fourth constriction (figure 1*b*) was similar, but included a straight section having parallel walls 60 mm apart and 0.5 m long (such that the total constriction length $L_c = 1.0$ m). Throughout this paper, we refer to the first three constrictions as 'short constrictions' and the latter as the 'long constriction'.

In each experiment, the tank was filled with freshwater to depth H. A sliding vertical barrier was inserted at the centre of the constriction and a measured quantity of salt was dissolved into the reservoir on the right-hand side of the barrier. The reservoirs were dyed with different colours to distinguish the layers for visualization, and both reservoirs were stirred thoroughly to ensure homogeneity. After adding the salt and dye there was a small difference between the free-surface heights on either side of the barrier. These heights were then adjusted to one of three different initial conditions:

(i) equal hydrostatic pressures at the bottom of the tank; (ii) equal pressures at mid-depth; or (iii) equal surface heights. Only the second case is expected to give purely baroclinic exchange. However, the results proved insensitive to these initial conditions. Before starting the exchange flow, the free-surface heights (h_1 and h_2) were measured using a digital micrometer gauge with an upward-pointing needle that approached the water surface from below. The densities were measured by analysing samples in an Anton Paar digital density meter.

The exchange flow was initiated by the smooth and rapid removal of the sliding barrier. Gravity currents formed on each side of the constriction and accommodated the exchange fluxes. The flow in the region of the constriction and near one end of the tank was imaged by separate cameras. The barrier was rapidly re-inserted into the constriction once the gravity currents had nearly reached the endwalls of the long tank (run times ranged from 15 s to 147 s).

After the exchange flow and prior to making any measurements, the experiment was left to stand for at least 2 h, long enough for all residual motions to decay, but too short for diffusion of salt to affect the density distribution on scales larger than 3 mm. During this time, the tank was sealed to minimize evaporation. Accurate density profiles were measured in both reservoirs using samples extracted simultaneously and spaced at 10 mm intervals throughout the water depth. Densities were measured to 0.001 kg m^{-3}. As measurements of the amount of mixing involved accurate calculation of the change of potential energy, precise measurements of the initial and final free-surface heights were also required: ± 0.01 mm errors in the surface height were sufficient to make the resulting uncertainties smaller than those from other sources.

Thirty experiments were run with the short constrictions, varying H (0.1, 0.2 or 0.3 m), b_o and the density difference $\Delta\rho = \rho_2 - \rho_1$ (across the range $0.001 \leqslant \Delta\rho/\rho_2 \leqslant 0.096$). Combinations of variable values were chosen so as to cover the maximum possible range of both aspect ratio H/L_c and Reynolds number $Re_H = \sqrt{g'H}H/\nu$ (equivalently expressed as a Grashof number, Hogg *et al.* 2001), where $g' = g\Delta\rho/\rho_2$ is the reduced gravity and ν is the kinematic viscosity. In addition, the results for the short constrictions were compared with those from nine experiments with the long constriction, in which H was fixed at 0.20 m.

3. Analysis

Measurements of the free-surface heights of the reservoirs before and after every exchange flow showed that the total volume of fluid in the reservoirs is conserved to within 0.01%. The density profiles $\rho_1'(z)$ and $\rho_2'(z)$ measured after the exchange flow can be used with conservation of mass (or salt) to derive expressions for the mass exchanged and the change in potential energy. The net rate of mass transport through the constriction is calculated with reference to a flow that is assumed to be purely baroclinic (i.e. the volume transport Q in each layer is equal and opposite). Net mass transport is then the product of Q with the density difference $\Delta\rho$ and is given by

$$M = \frac{A}{t}\int_0^{h_1'} (\rho_1'(z) - \rho_1)\,\mathrm{d}z, \tag{3.1}$$

where A is the cross-sectional area in each reservoir (which was uniform with height), t is the experimental run time and $z = 0$ at the base of the reservoirs.

The amount of mixing in the exchange flow can be obtained from the potential energy budget. The gravitational potential energy in each state sketched in figure 2 is

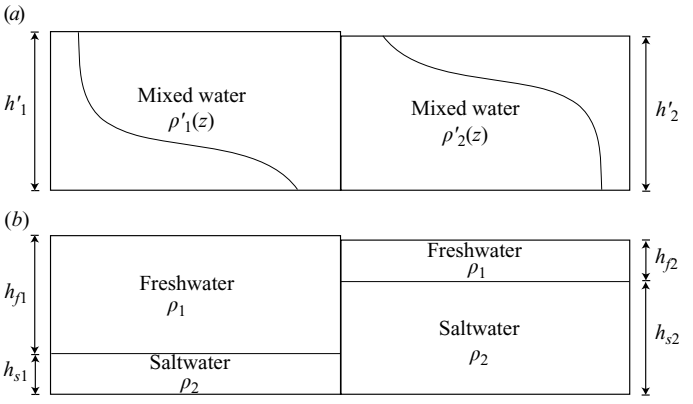

FIGURE 2. (*a*) The final state indicating the density profiles measured after the exchange flow. (*b*) The hypothetical minimum potential energy state resulting from exchange flow with no mixing. The initial state had density ρ_1, depth h_1 on the left and ρ_2, h_2 on the right.

given by

$$P = gA\int_0^{h'_1} \rho'_1(z)z\,\mathrm{d}z + gA\int_0^{h'_2} \rho'_2(z)z\,\mathrm{d}z. \tag{3.2}$$

In the initial state of two homogeneous reservoirs $\rho'_1(z)=\rho_1$, $\rho'_2(z)=\rho_2$, $h'_1=h_1$ and $h'_2=h_2$. In the final state (figure 2*a*), $P=P_f<P_i$, where subscripts f and i denote the final and initial states. However, P_f is greater than the potential energy P_h that would be present if no mixing occurred during the experiment. We determine P_h (figure 2*b*) by considering a hypothetical non-mixing flow having the same net mass transport as the actual experiment. Thus, we redistribute mass in the vertical to form a two-layer stratification and calculate the depths h_{s1} and h_{s2} of the hypothetical interfaces dividing fresh and salt water in each reservoir from

$$(\rho_2-\rho_1)h_{sj} = \int_0^{h'_j} (\rho'_j(z)-\rho_1)\,\mathrm{d}z \tag{3.3}$$

for $j=1,2$. This two-layer state has energy

$$P_h = gA\int_0^{h_{s1}} \rho_2 z\,\mathrm{d}z + gA\int_{h_{s1}}^{h'_1} \rho_1 z\,\mathrm{d}z + gA\int_0^{h_{s2}} \rho_2 z\,\mathrm{d}z + gA\int_{h_{s2}}^{h'_2} \rho_1 z\,\mathrm{d}z. \tag{3.4}$$

The increase in potential energy owing to mixing is given by the difference between the final and hypothetical (non-mixing) states: $P_m=P_f-P_h$. The available potential energy which is converted initially into kinetic energy (of both the mean flow and the turbulence) is the difference between the initial and hypothetical two-layer potential energy states: $APE=P_i-P_h$. We define mixing efficiency as the fraction of the total available potential energy released to the flow (and which we later argue goes into turbulent kinetic energy) that leads to an irreversible increase in the potential energy of the density distribution above the hypothetical two-layer state which would be achieved if there was no mixing. The efficiency η is then

$$\eta = \frac{P_m}{APE} = \frac{P_f-P_h}{P_i-P_h}. \tag{3.5}$$

Control experiments were carried out to examine the effects of the nonlinear equation of state of salt solutions, particularly at the larger concentration differences,

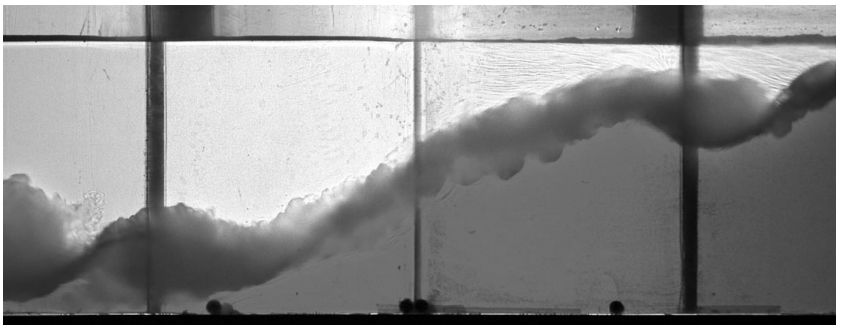

FIGURE 3. Intense mixing in the vicinity of the constriction in an experiment with $Re = 7.2 \times 10^4$, $b_o = 100\,\text{mm}$ (the shortest constriction), $H = 20\,\text{cm}$ and $\Delta\rho/\rho_2 = 6.7\%$.

where mixing tends to decrease the total volume and increase the internal potential energy, thus reducing the increase in gravitational potential energy owing to mixing. However, the influence on the calculated mixing efficiency was found to be smaller than 0.005, which is within the uncertainty of our measurements. Hence we have assumed in all calculations that the density depends linearly on salinity.

4. Results

4.1. *Qualitative observations*

The exchange flows in all cases led to shear instability and extensive mixing, particularly in the vicinity of the topographic constriction (see figure 3). Kelvin–Helmholtz billows grew to large amplitude within the constriction, but were not present beyond a hydraulic jump at each exit from the constriction. The mixed water was carried away from the constriction by gravity currents. Some mixing, but clearly a relatively small amount, took place at the gravity current head, and a very minor amount may have occurred in the stratified region above the currents along the length of the channel. After the barrier was replaced, a large-amplitude wave was reflected back from the far end of each reservoir and reflected again from the barrier, leading to a complex field of internal waves. The reflections and wave–wave interactions caused a further minor amount of mixing. Hence, this type of experiment cannot be used to quantitatively determine the relative amounts of mixing either at different locations or by the different processes. Rather the strength of the experiment is that it allows direct and precise measurements of the overall amount of mixing in the whole of the exchange flow.

Within the constriction, where the flow was subject to acceleration, billows and small-scale turbulence produced an interfacial region whose thickness was approximately 1/4 of the total water depth. Despite the globally unsteady nature of the 'dam-break' flow, that in the constriction was steady (apart from the initial slumping phase of the interface, which occupied only 10% of the available run time, and the low-mixing state after the barrier was replaced). In cases with smallest Reynolds numbers, the billows in the constriction were of comparable size but intermittent, and there appeared to be much less small-scale turbulence at the interface.

4.2. *Measured mixing efficiency*

Figure 4 shows the final density profiles for three experiments with different constriction widths, but the same values for all other variables including the same

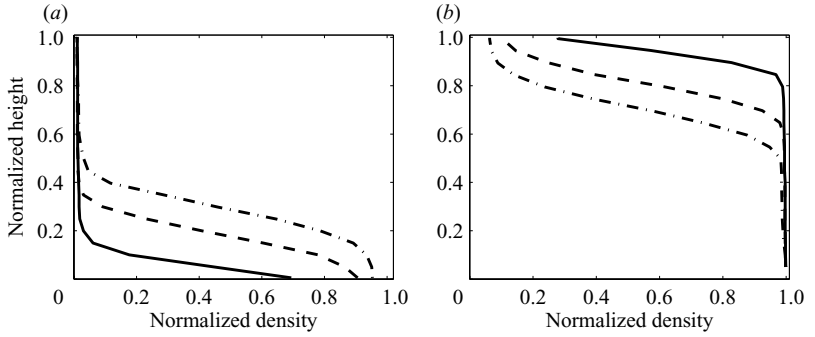

FIGURE 4. Examples of the final normalized density profiles $(\rho(z)-\rho_1)/(\rho_2-\rho_1)$ in the left (a) and right (b) reservoirs for three constriction widths. The cases shown had a run time $t=59\pm1$ s, $\Delta\rho/\rho_2=0.7\%$, $H=0.20$ m and $b_o=20$ mm (solid line), $b_o=60$ mm (dashed line) or $b_o=100$ mm (dashed-dotted line).

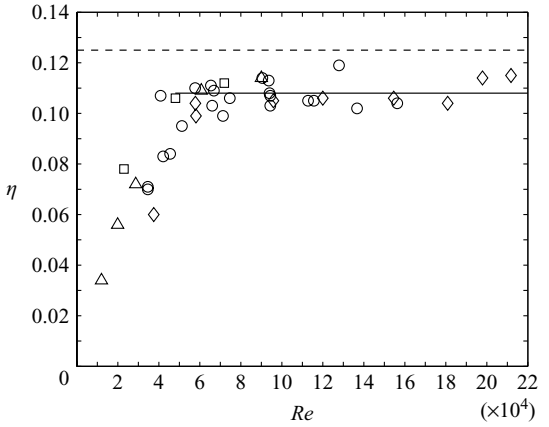

FIGURE 5. Measured mixing efficiencies η as a function of the horizontal Reynolds number Re for all experiments. Symbols indicate $b_o=20$ mm (○), 60 mm (△) and 100 mm (□) for short constrictions and $b_o=60$ mm (◇) for the long constriction. The dashed line shows the theoretical value ($\eta\approx0.125$) for mixing efficiency given by (4.8); the solid line describes the mean ($\eta=0.108$ with standard deviation 0.005) of the measured efficiencies for $Re\gtrsim5\times10^4$.

experimental run time. The net mass transport was greater in experiments with wider constrictions and we verified that, to leading order, it scaled with the ideal hydraulic prediction for the maximal exchange flux M_h, where $M_h=1/4\Delta\rho b_o g'^{1/2}H^{3/2}$ and the corresponding volume transport in each layer is $Q=M_h/\Delta\rho$. More precisely, the transport through all of the 'short' constrictions under all conditions was $M=(0.82\pm0.02)M_h$, consistent with the previous results for transport reduction owing to mixing. The transport through the 'long' constriction was $M=(0.70\pm0.01)M_h$, the smaller value being a result of energy loss in the long straight section, which had 'exit control points' at each end and the interface sloped between these points (Gu & Lawrence 2005). In this longer constriction, both mixing and friction are expected to play a role in reducing the transport.

The efficiencies (figure 5) indicate a constant value of $\eta=0.11$ (±0.01) for all experiments with sufficiently large Reynolds numbers, where the uncertainty quoted is twice the standard deviation of 0.005. Smaller efficiencies were found for small

Reynolds numbers. However, Re_H does not collapse these data, and there is a trend in the value of Re_H at which the efficiency reaches its asymptotic value. After exploring the roles of all parameters, we concluded that the measured mixing efficiencies at small Reynolds numbers are collapsed onto a single function only by the product of Re_H and L_c/H, which we write as the horizontal Reynolds number $Re = 0.5\sqrt{g'H}L_c/\nu$. The results are plotted in figure 5 as a function of Re and efficiencies reach an asymptote at $Re \gtrsim 5 \times 10^4$. We deduce that the relevant length scale for the Reynolds number is L_c, the distance over which intense mixing occurs, because at the smaller Reynolds numbers, billow growth was slower and the resulting turbulence more intermittent, so that for longer channels the instabilities have more time to complete irreversible mixing before collapsing and being swept out of the main mixing region. The smaller mixing efficiencies at smaller Re imply a relatively larger role of viscous dissipation of energy, which may take place increasingly from the mean flow rather than through turbulence.

The results of primary interest are those for large Reynolds numbers. Here, the efficiency does not depend on Reynolds number, or constriction width or length (noting that data for the long constriction are included in figure 5), nor does it depend on the aspect ratio H/L_c (which varied from 0.17 to 0.52). The latter point is consistent with scaling of the momentum equation, in which non-hydrostatic mean flow effects appear at order $(H/L_c)^2$, and with the previous experimental finding that non-hydrostatic effects at similar aspect ratios to those used here do not influence the transport (Zhu & Lawrence 1998). The efficiency (3.5) does not explicitly allow for dissipation on the sidewalls and bottom. However, the constant value found at large Re indicates that these effects are small.

Another parameter examined was the run time. In most cases, this was slightly less than the time for the gravity currents to reach the endwalls. However, additional runs with shorter times (data not included in figure 5) were carried out in order to examine the time-dependence of mixing. These confirmed that the rate of mixing was constant. This also confirms the contention that mixing associated with starting and ending the exchange flow (e.g. wave reflections and interactions) constitutes an insignificant contribution to the overall amount of mixing. Between 34% and 86% of the initial available potential energy was released during an experiment (i.e. before the currents reached the endwalls for the first time), the fraction increasing with constriction width. For the 20 mm constriction width, less than 6% of the energy released was present as kinetic energy of the mean flow at the moment the barrier was replaced, and therefore could not lead to significant additional mixing after the exchange was stopped.

4.3. *Theoretical prediction of mixing efficiency*

Following the methods outlined by Anati, Assaf & Thompson (1977) and Helfrich (1995), we assume that the flow initially accelerates until instability and turbulent mixing create an interfacial layer of thickness δ, after which the time-averaged gradients of density and velocity are constant (figure 6*a*). We further argue that the interfacial mixed layer is characterized by a marginally stable gradient Richardson number $Ri_g \approx 0.25$ so that, in a time-averaged sense, the mixing overturns can be maintained. Thus

$$Ri_g = \frac{N^2}{(\mathrm{d}u/\mathrm{d}z)^2} = \frac{g'\delta}{(\Delta U)^2} = \frac{\delta}{H}, \tag{4.1}$$

where $N = (g'/\delta)^{1/2}$ and $\mathrm{d}u/\mathrm{d}z$ are the buoyancy frequency and velocity gradient, respectively, in the interfacial mixed layer. The velocity difference across the mixed layer is ΔU and we have assumed that $\Delta U = (g'H)^{1/2}$ from the hydraulic solution.

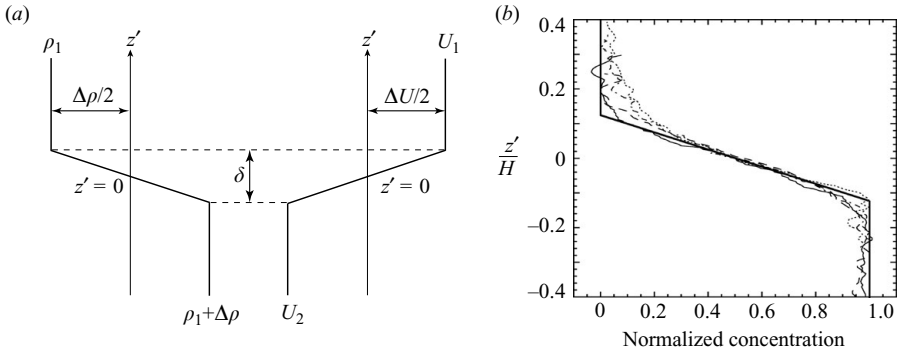

FIGURE 6. (*a*) A sketch of idealized time-averaged profiles of velocity and density in the interfacial mixed region of thickness δ. The centre of the mixed region is defined to be at height $z'=0$. (*b*) Measured profiles of normalized mean dye concentration for four experiments (0 corresponds to undyed water and 1 to the concentration in the dense reservoir). The dark solid line denotes the piecewise linear approximation with $\delta/H=0.25$ and matches the central gradient.

This prediction of the interface thickness is compared in figure 6(*b*) with profiles of time-averaged dye concentration near the centre of the contraction (obtained from an average of over 400 individual frames from videos of experiments in which dye was added only to the dense reservoir). The profiles show that mean interface thickness lies in the range $\delta/H=[0.23, 0.25]$, in accord with (4.1). This value is between $\delta/H\approx 0.2$ as discussed in Anati *et al.* (1977), based on a theoretical prediction for short straits, and $\delta/H\approx 0.3$ as used by Helfrich (1995), based on experimental measurements (Sherman, Imberger & Corcos 1978; Koop & Browand 1979).

The model mixed-layer density and velocity profiles $\rho(z')=-\Delta\rho z'/\delta$ and $u(z')=\Delta U z'/\delta$, where the vertical coordinate z' is centred on the middle of the mixed layer, are assumed to have the same thickness δ (Thorpe 1973). An assumption of no net flux of energy into or out of the layer can be used to calculate the change in potential and kinetic energies of the interfacial mixed layer relative to those that would exist in an inviscid and non-mixing two-layer flow. The potential energy in the interfacial mixed layer is given by

$$P_{int}=\int_{-\delta/2}^{\delta/2}\rho g z'\,\mathrm{d}z'=-\tfrac{1}{12}\Delta\rho g\delta^2, \tag{4.2}$$

which we compare with the potential energy in the non-mixing two-layer flow,

$$P_{tl}=\int_{-\delta/2}^{0}(\rho_1+\Delta\rho)gz'\,\mathrm{d}z'+\int_{0}^{\delta/2}\rho_1 g z'\,\mathrm{d}z'=-\tfrac{1}{8}\Delta\rho g\delta^2. \tag{4.3}$$

Thus, the increase in potential energy in the mixed layer owing to mixing is

$$\Delta P=P_{int}-P_{tl}=\tfrac{1}{24}\Delta\rho g\delta^2. \tag{4.4}$$

The mean kinetic energy in the interfacial mixed layer is given by

$$K_{int}=2\int_{0}^{\delta/2}\tfrac{1}{2}\overline{\rho}u^2\,\mathrm{d}z'=\tfrac{1}{24}\overline{\rho}(\Delta U)^2\delta, \tag{4.5}$$

where $\overline{\rho}$ is the mean density and we have invoked symmetry in the mixed layer. In the non-mixing case, the kinetic energy in the same region would be

$$K_{tl} = 2\int_0^{\delta/2} \frac{1}{2}\overline{\rho}\left(\frac{\Delta U}{2}\right)^2 \mathrm{d}z' = \frac{1}{8}\overline{\rho}(\Delta U)^2\delta. \tag{4.6}$$

The difference between the kinetic energies of the non-mixing and actual states is indicative of the turbulent kinetic energy released from the mean flow in the mixed layer, and is given by

$$\Delta K = K_{tl} - K_{int} = \tfrac{1}{12}\overline{\rho}(\Delta U)^2\delta. \tag{4.7}$$

Using the definition (3.5), an estimate of the mixing efficiency becomes

$$\eta = \frac{\Delta P}{\Delta K} = \frac{1}{2}\frac{g'\delta}{(\Delta U)^2} = \frac{1}{2}Ri_g. \tag{4.8}$$

If the time-averaged Ri_g tends to a mean value 0.25 ± 0.05, the mixing efficiency becomes $\eta \approx 0.125 \pm 0.025$. This limit is shown in figure 5 (dashed line), and is a good approximation to the measured efficiencies in cases where Re is sufficiently large.

5. Discussion

The measured mixing efficiency is $\eta = 0.11$ (± 0.01) for all geometric configurations tested here, provided only that the horizontal Reynolds number, $Re > 5 \times 10^4$. Our aim was to determine the total amount of mixing and the corresponding bulk mixing efficiency for hydraulically controlled exchange flows. The measurements incorporate all sources of mixing in the experiment, including shear instability and hydraulic jumps associated with the constriction, as well as gravity currents, wave reflections and wave–wave interactions that are associated with the strait-basin system. However, the most visibly intense mixing takes place in the constriction and near its exits, and the energy available to drive mixing is largely depleted by the time the currents reach the far ends of the long channel. Hence, we suggest that the efficiency measured here will more generally characterize mixing in exchange flows. As the development of Kelvin–Helmholtz billows in the strait appears to be the dominant mechanism responsible for mixing, the measured efficiency may also be characteristic of a broader range of two-layer stratified shear flows. The scaling analysis leading to (4.8) makes no assumption about hydraulic control or the geometry.

Our definition of mixing efficiency is similar to that used by Caulfield & Peltier (2000) and Peltier & Caulfield (2003) for numerical experiments in stratified shear flow, although those authors did not measure the potential energy of the mean flow in a manner suitable for direct comparison. Instead, they defined a bulk efficiency as the ratio of the time-integrated mixing and dissipation rates, and found $\eta \approx 0.15$, only slightly greater than the present result.

The application of the results to ocean strait dynamics is straightforward. It is clear that ocean straits (and estuarine exchange flows) will tend to the large Re limit. The experiments also show that the efficiency of mixing, unlike the mass transport, is not influenced by frictional effects. It follows that mixing efficiencies associated with such flows will approach the upper limit shown here. However, the caveat on these results is that we are yet to complete a study of the effect of bottom topography (sills and deep basins) on mixing efficiency.

The results also provide information which may be applied to a major problem in oceanography – the energetics of the overturning circulation. Numerous studies (see

Wunsch & Ferrari 2004) have applied a standard assumption that approximately 20% of the bulk kinetic energy in the abyssal ocean is converted into mixing, irrespective of the mixing process. The smaller asymptotic mixing efficiency of 11% found here, along with the computational results of Caulfield & Peltier (2000) and Peltier & Caulfield (2003), raise the possibility that average efficiencies in the ocean may not be as large as assumed. Resolving this issue is beyond the scope of the current paper, but our results indicate that the bulk mixing efficiency in stratified flows is not yet understood.

T.P. was funded by an AusAID Scholarship from the Australian Government, the work was partially supported by an ARC Discovery Grant (DP0664115) and A.M.H. was supported by an Australian Postdoctoral Fellowship (DP0449851). We thank Tony Beasley for technical support in constructing the apparatus.

REFERENCES

Anati, D. A., Assaf, G. & Thompson, R. O. R. Y. 1977 Laboratory models of sea straits. *J. Fluid Mech.* **81**, 341–351.

Bryden, H. L. & Nurser, A. J. G. 2003 Effects of strait mixing on ocean stratification. *J. Phys. Oceanogr.* **33**, 1870–1872.

Caulfield, C. P. & Peltier, W. R. 2000 The anatomy of the mixing transition in homogeneous and stratified free shear layers. *J. Fluid Mech.* **413**, 1–47.

Gregg, M. C. & Özsoy, E. 2002 Flow, water mass changes, and hydraulics in the Bosphorus. *J. Geophys. Res.* **107** (C3), 10.1029/2000JC000485.

Gu, L. & Lawrence, G. A. 2005 Analytical solution for maximal frictional two-layer exchange flow. *J. Fluid Mech.* **543**, 1–17.

Helfrich, K. L. 1995 Time-dependent two-layer hydraulic exchange flow. *J. Phys. Oceanogr.* **25**, 359–373.

Hogg, A. M., Ivey, G. N. & Winters, K. B. 2001 Hydraulics and mixing in controlled exchange flows. *J. Geophys. Res.* **106**, 959–972.

Koop, C. G. & Browand, F. K. 1979 Instability and turbulence in a stratified fluid. *J. Fluid Mech.* **93**, 135–160.

Lawrence, G. A. 1990 On the hydraulics of Boussinesq and non-Boussinesq two-layer flows. *J. Fluid Mech.* **215**, 457–480.

Munk, W. & Wunsch, C. 1998 Abyssal recipes II: energetics of tidal and wind mixing. *Deep-Sea Res.* I **45**, 1977–2010.

Peltier, W. R. & Caulfield, C. P. 2003 Mixing efficiency in stratified shear flows. *Annu. Rev. Fluid Mech.* **35**, 135–167.

Sherman, F. S., Imberger, J. & Corcos, G. M. 1978 Turbulence and mixing in stably stratified waters. *Annu. Rev. Fluid Mech.* **10**, 267–288.

Thorpe, S. A. 1973 Experiments on instability and turbulence in a stably stratified shear flow. *J. Fluid Mech.* **61**, 731–751.

Winters, K. B. & Seim, H. E. 2000 The role of dissipation and mixing in exchange flow through a contracting channel. *J. Fluid Mech.* **407**, 265–290.

Wood, I. R. 1970 A lock exchange flow. *J. Fluid Mech.* **42**, 671–687.

Wunsch, C. & Ferrari, R. 2004 Vertical mixing, energy, and the general circulation of the oceans. *Annu. Rev. Fluid Mech.* **36**, 281–314.

Zhu, D. Z. & Lawrence, G. A. 1998 Non-hydrostatic effects in layered shallow water flows. *J. Fluid Mech.* **355**, 1–16.